Editors' Suggestion

Disordered monitored free fermions

Marcin Szyniszewski [1,*] Oliver Lunt, [1,2,3] and Arijeet Pal [1]

[1] *Department of Physics and Astronomy, University College London, Gower Street, London, WC1E 6BT, United Kingdom*
[2] *Department of Physics, King's College London, Strand, London, WC2R 2LS, United Kingdom*
[3] *School of Physics & Astronomy, University of Birmingham, Birmingham, B15 2TT, United Kingdom*

(Received 10 February 2023; revised 26 September 2023; accepted 27 September 2023; published 17 October 2023)

Scrambling of quantum information in unitary evolution can be hindered due to measurements and localization, which pin quantum mechanical wave functions in real space, suppressing entanglement in the steady state. In monitored free-fermionic models, the steady state undergoes an entanglement transition from a logarithmically entangled critical state to area law. However, disorder can lead to Anderson localization. We investigate free fermions in a random potential with continuous monitoring, which enables us to probe the interplay between measurement-induced and localized phases. We show that the critical phase is stable up to a finite disorder, and the criticality is consistent with the Berezinskii-Kosterlitz-Thouless universality. Furthermore, monitoring destroys localization, and the area-law phase at weak dissipation exhibits power-law decay of single-particle wave functions. Our work opens an avenue to probe this phase transition in electronic systems of quantum dot arrays and nanowires and allow quantum control of entangled states.

DOI: 10.1103/PhysRevB.108.165126

I. INTRODUCTION

The preservation of information in many-body quantum systems poses a substantial challenge in quantum computing. Generically, as quantum systems evolve in time, any initial quantum information is scrambled throughout the system, becoming inaccessible through local measurements, leading to thermalization. In recent years, it has become clear that there are quantum systems that can fail to thermalize, the most prominent example being the phenomenon of many-body localization (MBL) [1–5]. In such systems, quantum information remains accessible via local measurements even at long times and preserves correlations in the initial state. The MBL phase transition separating localized and chaotic phases of matter is characterized by a singular change in the entanglement properties of the system.

Entanglement phase transitions can also occur in quantum trajectories of open quantum systems [6–8]. The transition occurs due to a competition between measurements and unitary evolution, hence the name measurement-induced entanglement transition (MIET). This type of phase transition has been of interest in many recent studies [9–127]. Typically, one considers a quantum circuit with unitary gates interspersed with local measurements at random locations. The transition between the volume-law and the area-law phase occurs at a finite measurement probability and is known to occur in a wide variety of systems: unitaries can be randomly drawn either from the Haar measure or the Clifford group [6–9], or a Hamiltonian evolution of interacting systems [45–49], while the measurements can be chosen to be projective or weak. The universal properties of the MIET in random unitary circuits have similarities with those of percolation, though there appear to be some differences in surface critical behavior [8,11,16–19,21].

Intriguingly, the phase diagram changes significantly for a free-fermionic system [32–44]. The volume-law entangled steady state for nonzero measurement probability is fragile due to its lack of multipartite entanglement in free-fermion systems [32,33]. For a range of measurement probabilities, an extended critical phase with logarithmic growth of entanglement and conformal symmetry emerges [33]. Beyond a critical measurement probability, the systems transition into

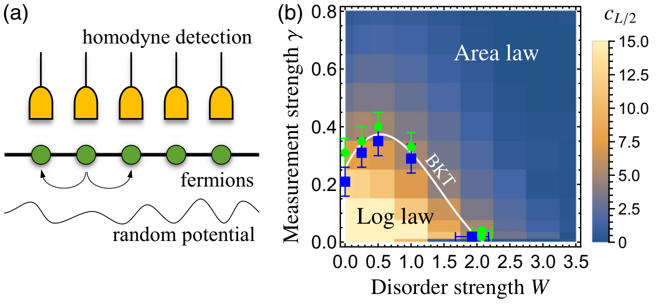

FIG. 1. (a) Sketch of disordered monitored free fermions. (b) Phase diagram. The density plot shows the effective central charge estimate $c_{L/2}$. Data collapses of half-chain entanglement entropy (green circles) and central charge (blue squares) are used to estimate the transition boundary (solid line).

*mszynisz@gmail.com

an area-law phase. A substantial amount of evidence implies that this MIET is within the Berezinskii-Kosterlitz-Thouless (BKT) universality class [33,34], which puts it in a distinct class from random unitary circuits. Recent developments also suggest that the transition happens due to pinning of the wave-function trajectory to the eigenstates of the measurement operator [34].

However, several important questions relating to the robustness of the critical logarithmic phase remain unanswered. For example, the logarithmic phase remaining stable against breaking of the continuous U(1) symmetry, for particle number conservation, to a discrete $\mathbb{Z}_2$ fermion parity symmetry is associated with continuous replica symmetry breaking which does not appear to have a physical analog [31,34,38,60]. For free-fermionic systems in one dimension (1D), it is particularly interesting to ask about robustness to quenched disorder. For a noninteracting Hamiltonian, arbitrarily weak disorder localizes the single-particle modes in 1D, a phenomenon known as Anderson localization [128–130]. The role of measurements can destroy the localized phase at intermediate couplings while facilitating localization into product states at strong coupling. The competition between measurements and quenched disorder can result in a rich phase structure for an entanglement transition and is also relevant for observing the critical to area-law phase transition in an experimental setting. Disorder plays an essential role in a system of electrons in quantum dot arrays and nanowires where these phenomena can be explored.

Motivated by this question, in this paper, we investigate the impact of quenched disorder on the measurement-induced transition in a 1D free-fermion system. A careful analysis of the entanglement entropy and central charge leads us to a phase diagram in terms of measurement strength γ and disorder W [see Fig. 1(b)] which exemplifies the robustness of the logarithmic phase and the relationship between Anderson localized and measurement-induced area-law phases of noninteracting electrons.

II. MODEL

We consider spinless fermions hopping in a 1D lattice with a random potential, subject to continuous measurements [see Fig. 1(a)]:

$$H = \sum_{i=1}^{L}(c_i^\dagger c_{i+1} + \text{H.c.}) + \sum_{i=1}^{L} h_i n_i, \tag{1}$$

where the random potential is distributed uniformly $h_i \in [-W, W]$ with disorder strength W. The system is initially set to a separable Néel state. The evolution is implemented using the stochastic Schrödinger equation:

$$d|\psi(t)\rangle = -iH\,dt|\psi(t)\rangle - \frac{\gamma\,dt}{2}\sum_i (n_i - \langle n_i\rangle)^2|\psi(t)\rangle + \sum_i (n_i - \langle n_i\rangle)d\eta_i^t|\psi(t)\rangle, \tag{2}$$

which describes the continuous monitoring of particle number operator n_i on each site, with measurement strength γ [32]. The Itô increments $d\eta_i^t$ have zero mean and variance of $\gamma\,dt$ (see Appendix for details).

We monitor each quantum trajectory, characterized by a set of measurement outcomes for a single realization of the random potential; the results are then averaged over multiple trajectories. Importantly, this provides access to averages of nonlinear functions of the reduced density matrix, which in turn allow us to capture the entanglement phase transition. Specifically, we use the von Neumann entropy, a measure of entanglement between subsystem A and its complement, defined as $S = -\text{tr}(\rho_A \ln\ \rho_A)$, where ρ_A is the reduced density matrix of A. Here, S is initially zero for a separable state and grows in time, saturating near a fixed point S_∞ at long times, estimated as time average after saturation $S_\infty = \lim_{\Delta T\to\infty}\int_{t_{\text{sat}}}^{t_{\text{sat}}+\Delta T} S(t)dt/\Delta T$. Finally, S_∞ is averaged over trajectories, giving $\bar{S}$.

Entanglement phase transitions can be directly observed by monitoring how $\bar{S}$ changes with the system size L. However, even in free-fermion circuits, where we can access larger system sizes, finite-size effects are significant and impede our analysis. Special care needs to be taken for the critical phase, where both $\bar{S}$ and the correlation length ξ diverge logarithmically with L—extraction of the critical point is difficult for phase transitions with slowly diverging length scales [33]. This critical phase is expected to be described by a 1+1D nonunitary conformal field theory (CFT) with periodic boundaries, with

$$\bar{S}(l, L) = \frac{c}{3}\ln\left(\frac{L}{\pi}\sin\frac{\pi l}{L}\right) + s_0, \tag{3}$$

where l is the length of the subsystem A, c is the effective central charge of the nonunitary CFT, and s_0 is the residual entropy. For large enough systems, c is expected to be zero in the area-law phase and finite in the log phase and thus can be used as a transition diagnostic.

III. RESULTS

A. Phase diagram

Using the results for $\bar{S}(L/2, L)$ as a function of L, we perform a fit to Eq. (3) and obtain a central charge estimate $c_{L/2}$. This allows us to draw the dependence of $c_{L/2}$ on the measurement strength γ and the disordered field strength W—see Fig. 1(b). The central charge remains nonzero at low values of γ and W, implying the existence of the critical phase. However, at large values of either γ or W, $c_{L/2}$ stays close to zero, a signature of the area law. This suggests that the logarithmic phase survives the introduction of the random disordered field, and only when the field is strong enough ($W \gtrsim 3.5$), the phase breaks down.

Estimation of the precise phase boundary is, however, difficult, as $c_{L/2}$ does not decay sharply to zero. Large finite-size effects necessitate a scaling analysis, which we perform in the next sections. Nonetheless, two peculiar features can immediately be seen in the density plot in Fig. 1(b): for small W, there is nonmonotonic behavior of the phase boundary [see Fig. 2(a)]; and for small γ, the density plot shows a rapid change of $c_{L/2}$ for $\gamma = 0$ (Anderson localized) vs when γ is finite [see Fig. 2(b)].

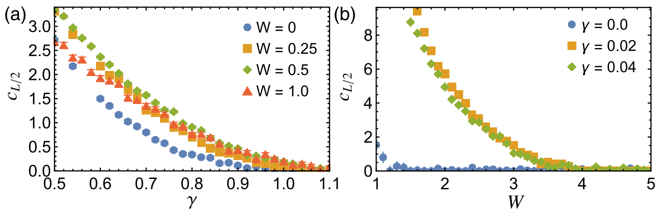

FIG. 2. Effective central charge estimate $c_{L/2}$, calculated using half-chain entanglement entropy (a) for small values of W and (b) for small values of γ.

B. Survival of the BKT universality class

We firstly discuss the case of small disorder strength. For the clean system ($W = 0$), we can fully reproduce existing results [32,33]. Importantly, Ref. [33] provides numerical evidence of the BKT universality class, for which the half-chain entropy can be collapsed using [131]

$$\bar{S}(L/2, L, \gamma) - \bar{S}\big(L/2, L, \gamma_c^{\bar{S}}\big) = F\big[\big(\gamma - \gamma_c^{\bar{S}}\big)(\ln L)^2\big], \quad (4)$$

where $\gamma_c^{\bar{S}}$ is the critical point; the optimal collapse gives $\gamma_c^{\bar{S}} \approx 0.31$. Another estimate comes from investigating c as a function of system size L. To do this, one extracts $c(L)$ for one specific L by fitting the entropy results for different bipartitions to Eq. (3). Then the $c(L)$ data can be collapsed according to [33]

$$c(L)\gamma g(L) = \tilde{F}\left[\ln L - \frac{\alpha}{\sqrt{\gamma - \gamma_c^{c(L)}}}\right], \quad (5)$$

which yields $\gamma_c^{c(L)} \approx 0.21$. The scaling function $g(L) = [1 + 1/(2\ln L - \beta)]^{-1}$ [33,131–133]. Although the two estimates have substantial error bars ($\approx$0.05), both are much lower than estimate based on $c_{L/2}$, where the transition would rather be expected at $\gamma_c^{c_{L/2}} \approx 0.8$ [cf. Fig. 2(a)]. This strongly suggests that $c_{L/2}$ cannot provide a good estimate of the transition point due to finite-size effects, and data collapses of $\bar{S}$ and $c(L)$ are needed instead.

Armed with this knowledge, we introduce a small amount of disorder ($W = 0.25, 0.5, 1.0$) [133]. The results for the half-chain entropy and the central charge are shown in Figs. 3(a) and 3(c). Judging from $\bar{S}(L/2)$, the corresponding transition region where the entropy starts deviating significantly from a $\ln(L)$ behavior for large L is $0.3 \lesssim \gamma_c \lesssim 0.37$ for $W = 0.5$. We also perform the data collapse for $\bar{S}(L/2)$ and $c(L)$, shown in Figs. 3(e) and 3(g), finding $\gamma_c^{\bar{S}} \approx 0.40$ and $\gamma_c^{c(L)} \approx 0.35$ for $W = 0.5$. All performed data collapses are of reasonably good quality, which suggests that the BKT universality class of the transition is preserved in the presence of weak disorder. This is consistent with the idea that the relevant symmetry is the continuous replica symmetry, which should be preserved if the system is still free fermionic [31,34,60].

This result is corroborated further by the behavior of the connected correlation function $\bar{C}(r) = \overline{\langle n_i\rangle\langle n_{i+r}\rangle - \langle n_i n_{i+r}\rangle}$ [see Figs. 4(a) and 4(b)], which decays algebraically as $\sim r^{-2}$ in the critical phase, like the clean system [33]. Deep within the area law, the correlations decay more rapidly, as expected,

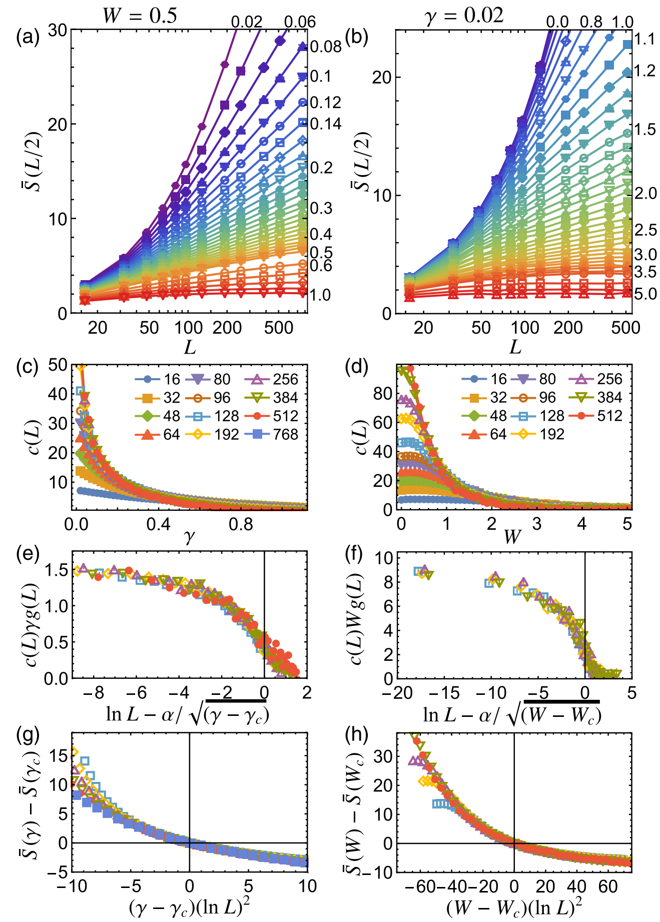

FIG. 3. Behavior for small W (left plots) and small γ (right plots). (a) and (b) Half-chain entropy $\bar{S}(L/2)$ for different values of the measurement strength γ or disorder strength W (see labels on the right). (c) and (d) Central charge $c(L)$ as a function of γ (or W) and system size L. Data collapses for (e) and (f) $c(L)$ and (g) and (h) $S(L/2)$. Legend from (c) and (d) applies in (e)–(h).

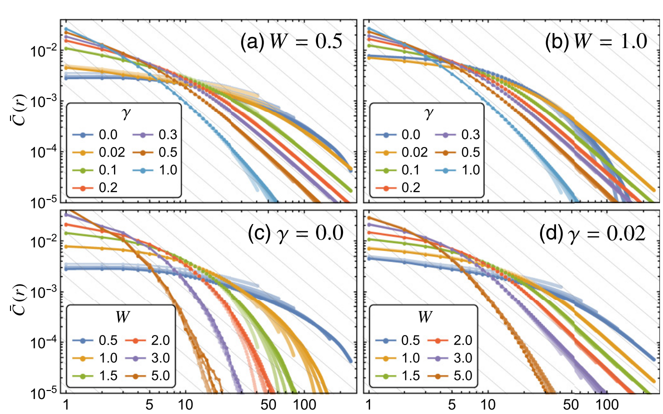

FIG. 4. Connected correlation function $\bar{C}(r)$ for constant disorder strength (a) $W = 0.5$, (b) $W = 1.0$, and constant measurement strength (c) $\gamma = 0.0$, (d) $\gamma = 0.02$. Plot opacity indicates the system size ($L = 128, 196, 256, 384, 512$, and 768). Gray lines show the algebraic decay of $\sim r^{-2}$ expected for the critical phase.

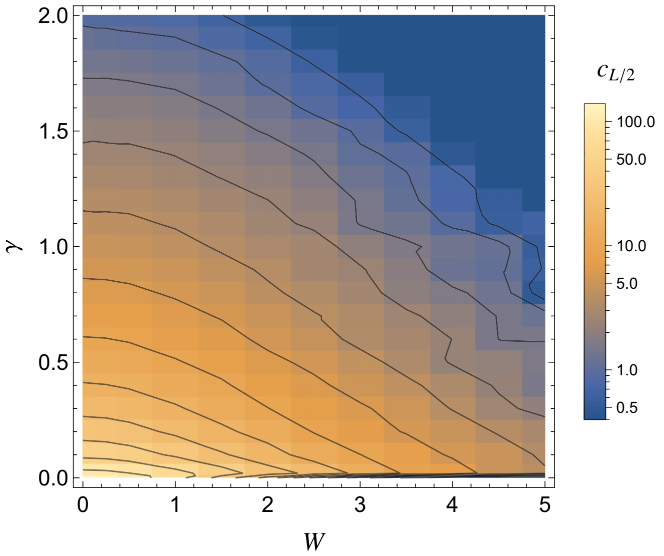

FIG. 5. Central charge as a function of measurement strength γ and disorder W for a system with additional next-nearest-neighbor interactions.

while for the exceptional point $\gamma = 0$, exponential decay is present.

Interestingly, for $W = 0.5$, all collapses yield γ_c estimates which are higher than those for both $W = 0$ and 1; this implies that the nonmonotonicity of the phase boundary near small W is a physical phenomenon and that introduction of weak disorder shifts the transition point γ_c to higher values. This behavior seems similar to the one observed in interacting models [89], where a small amount of noise facilitated entanglement spreading and extended the volume law. Here, a small amount of disorder stabilizes the logarithmic phase, as the observed values of $c(L)$ appear to be higher [see Fig. 2(a)]. Alternatively, a weak disordered field slightly impedes the ability of measurements to pin the wave function trajectory to the eigenstates of the measurement operator, so that the area law occurs at higher γ_c.

Since the entanglement transition is a direct result of the competition between the unitary evolution and measurements, we believe that this nonmonotonic behavior is tightly connected to the speed of entanglement spreading dictated by the hopping term. For this model, this speed seems low enough that the introduction of a small amount of disorder scrambles the information more efficiently, pushing γ_c to higher values. We test this hypothesis by adding next-nearest-neighbor interactions to the Hamiltonian:

$$H = \sum_i (c_i^\dagger c_{i+1} + c_i^\dagger c_{i+2} + \text{H.c.}) + \sum_i h_i n_i, \qquad (6)$$

which should increase the entanglement speed induced by the hopping terms. We find that the nonmonotonicity in the phase diagram is absent (see Fig. 5), as expected. This suggests that the next-nearest-neighbor interactions increase the entanglement speed enough, so that it is no longer impacted by a small disorder.

We would also like to comment on the recent results of Ref. [134], which put into question the existence of the critical phase in the clean model. The nonmonotonic behavior observed in the disordered free-fermion system studied here implies that the disorder may stabilize the critical phase, even if it is absent in the clean case, signifying the presence of the measurement-induced transition for a finite disorder strength.

C. Destruction of Anderson localization

We now discuss the topic of small measurement strengths. For $\gamma = 0$, the system becomes an Anderson insulator and exhibits an area law for any finite W. Below $W \lesssim 1.1$, finite-size effects cause finite $c_{L/2}$: localization length ξ in the Anderson model is inversely proportional to W^2 [135], and ξ becomes comparable with the considered system sizes when $c_{L/2}$ becomes nonzero. This should, however, not be an issue for larger γ, as the characteristic length ξ is affected by both the disorder and the measurements.

At very small but nonzero values of $\gamma = 0.02, 0.04$ [133], we observe an abrupt change to the localized behavior. Here, $\bar{S}(L/2)$ results suggest that a logarithmic dependence on the system size is present for small W [Fig. 3(b)], with the crossover to the area-law scaling at $\sim 1.5 \lesssim W \lesssim 2.5$. We pinpoint the transition, extracting $W_c^{\bar{S}} \approx 2.1$ and $W_c^{c(L)} \approx 1.9$ for $\gamma = 0.02$. Importantly, W_c is large enough not to be impacted by the characteristic length ξ being comparable with L, and therefore, we believe the observed transition to be physical. Our results suggest the BKT universality class is preserved for the whole transition boundary in Fig. 1(b). Furthermore, the connected correlators change their behavior between $\gamma = 0$ and 0.02 [see Figs. 4(c) and 4(d)] from faster than algebraic to $1/r^2$ decay for $W < W_c$, indicating emergence of the conformal phase.

We thus conclude that Anderson localization is immediately broken for any finite value of γ, and the critical phase reappears in the phase diagram. This phenomenon most likely occurs due to measurements impeding interference through impurity scattering—even very weak measurements change the scattered fermionic modes, and destructive interference is not possible, rendering the mechanism behind Anderson localization disrupted. A similar mechanism occurs when inelastic scattering is introduced to an Anderson-localized medium, where the phase coherence between outgoing and ingoing modes is disrupted [136]. Whether the measurements force the system into the critical phase or the area law depends on the shape of localized single-particle orbitals $|\psi_i|^2$ at $\gamma = 0$ [see Figs. 6(a) and 6(b)], which can be read off from the Slater determinant. At large disorder, the orbitals decay rapidly, and the overlap between their envelopes is negligible. The measurements have little impact, only sharpening the orbitals at their localization centers, and the area law is preserved. At small disorder, the orbitals are broad, and their envelopes substantially overlap with each other. The measurements effectively introduce scrambling between them, which leads to a delocalized behavior and the critical phase. This very simple picture would suggest that the transition happens approximately when $\xi \sim 1$, while our numerical results reveal a slightly larger critical localization length of $\xi \sim 24/W_c^2 \approx 6$ [135].

Furthermore, we find a clear distinction between the Anderson-localized area law and the measurement-induced area law for $\gamma > 0$. The former is characterized by

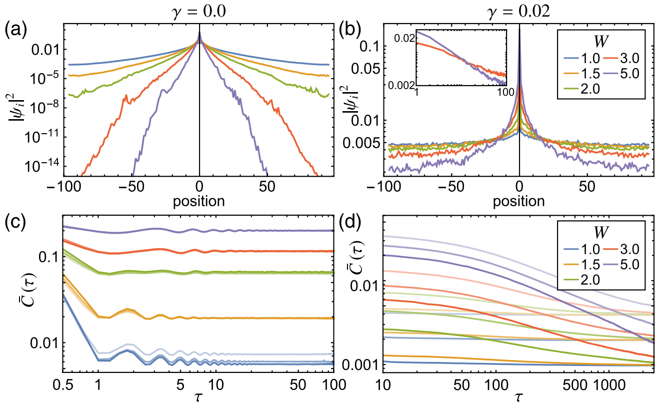

FIG. 6. (a) and (b) Averaged steady-state fermion orbitals $|\psi_i|^2$ for $L = 192$ for different values of W. Inset in (b) shows the log-log plot, suggesting power-law decay. (c) and (d) Autocorrelation functions $\bar{C}(\tau)$ for different values of W and system sizes $L = 128$ (lighter), 256, and 512 (darker). Left plots: $\gamma = 0$; right plots: $\gamma = 0.02$.

exponential decay of the orbitals, while the latter exhibits power-law localization, $|\psi_i(x)|^2 \sim x^{-\alpha}$ [inset in Fig. 6(b)] [133]. Autocorrelation functions $\bar{C}(\tau)$ [Figs. 6(c) and 6(d)] also showcase this difference. For $\gamma = 0$, $\bar{C}(\tau)$ quickly saturates to a constant and does not decay. However, for $\gamma > 0$, $\bar{C}(\tau)$ plateaus for a long period ($\tau \sim 100$), and eventually decays due to the disruption from measurements to a minimum value of $1/(2L)$. The plateau size depends on γ, where for large γ, the decay begins earlier. The decay itself seems to be approximately a power law, with larger systems taking more time to reach the minimum value.

IV. CONCLUSIONS

The results presented in this paper show the nontrivial interplay between Anderson localization and continuous measurements. We convincingly demonstrate that the entanglement phase transition from the critical phase with conformal symmetry to the area-law phase survives the introduction of quenched disorder. Moreover, the universality class of this transition also seems to be preserved, which strongly suggests that the logarithmic phase is stable to weak perturbations. We also find that a small amount of disorder can help stabilize the critical phase. Gathering all our data from the collapse of entanglement entropy and effective central charge, we estimate the true transition boundary between the logarithmic and area-law phases [solid line in Fig. 1(b)]. In general, our results convincingly suggest the conformal phase and free-fermion MIETs are viable for experimental probing in systems such as nanowires and quantum dot arrays, which host Anderson localization along with implementation of local measurements [137].

We find that an introduction of monitoring in the Anderson-localized model results in an instant destruction of the localization for weak disorder. The delocalization results from the destruction of the coherent processes leading to a liquid state, although, at sufficiently large disorder, the system transitions into an area-law state which is markedly distinct from Anderson localization as the orbitals exhibit a power-law decay in space instead of exponential. The temporal behavior of the autocorrelations exhibits parametrically longer decay time scales compared with Anderson localization. There are several interesting directions for future work emerging from our results. The role of interactions in the logarithmic phase and its relationship to MBL remains a challenging open problem. The fate of the critical phase for integrable models which do not map to free fermions could also provide classes of measurement-induced criticality.

All relevant data present in this publication can be accessed at [138].

ACKNOWLEDGMENTS

We thank Romain Vasseur, Sebastian Diehl, Alessandro Romito, Paul Pöpperl, Igor Poboiko, and Igor Gornyi for useful discussions. A.P. and M.S. were funded by the European Research Council under the European Union's Horizon 2020 research and innovation programme (Grant Agreement No. 853368). O.L. was supported by UKRI Grant No. MR/T040947/1. The authors acknowledge the use of the UCL Myriad High Performance Computing Facility and associated support services in the completion of this paper.

APPENDIX: METHODOLOGY

The evolution considered in this paper preserves particle number and can be efficiently simulated with a method based on the stochastic Schrödinger equation [32]. The wave function is a pure Gaussian state of N particles on L sites and can be described by an $N \times L$ matrix U:

$$|\psi\rangle = \prod_{k=1}^{N}\left(\sum_{j=1}^{L} U_{jk} c_j^\dagger\right)|0\rangle, \tag{A1}$$

where $c_j^\dagger$ are the fermionic creation operators, and $|0\rangle$ is the vacuum state. Physically, U is a matrix of fermion orbitals (single-particle wave functions), and $\det(U)$ is a Slater determinant. In this paper, we always consider a case of half-filling and start the evolution from a Neél state.

The measurements and time evolution are implemented using the stochastic Schrödinger equation, where a monitoring of an operator O is done by evolving the wave function according to

$$d|\psi(t)\rangle = -iHdt|\psi(t)\rangle + \mathcal{M}|\psi(t)\rangle, \tag{A2}$$

where the measurement operator is $\mathcal{M} = [(O - \langle O\rangle_t)d\eta_t - \frac{\gamma}{2}(O - \langle O\rangle_t)^2 dt]$, with η_t a Wiener process and γ the measurement strength/rate. We will measure operator $n_i = c_i^\dagger c_i$ on every site. This evolution can be approximated by trotterization $|\psi(t+dt)\rangle \approx e^{\mathcal{M}} e^{-iHdt}|\psi(t)\rangle$.

Importantly, this corresponds to an evolution of the matrix U that fully describes the Gaussian state:

$$U(t+dt) = e^{M} e^{-ihdt} U(t), \tag{A3}$$

where M is a matrix with elements $M_{ij} = \delta_{ij}[\eta_i + (2\langle n_i\rangle - 1)\gamma dt]$, and h corresponds to the free-fermion Hamiltonian $H = \sum_i c_i^\dagger c_{i+1} + \text{H.c.}$, and has elements $h_{ij} =$

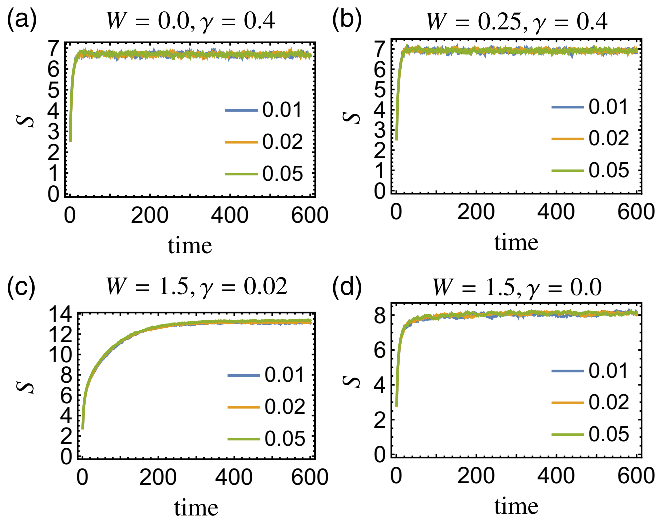

FIG. 7. Averaged entanglement entropy S as a function of time for four values of disorder W and measurement strength γ: (a) $W = 0.0$, $\gamma = 0.4$, (b) $W = 0.25$, $\gamma = 0.4$, (c) $W = 1.5$, $\gamma = 0.02$, and (d) $W = 1.5$, $\gamma = 0.0$. The system size is $L = 256$. Different colors signify the time steps $dt = 0.01$, 0.02, and 0.05. The curves collapse well for all used timesteps. At long times, entropy reaches the saturation value S_∞.

$\delta_{i,j+1} + \delta_{i,j-1} + h_i\delta_{i,j}$. After each timestep dt, the wave function needs to be properly normalized, which can be done by a QR decomposition of matrix $U(t + dt) = QR$, and setting the new matrix U to be Q.

Figure 7 shows that setting $dt = 0.05$ is enough to describe the continuous-time regime, and we find that lowering dt does not change our results within the statistical error bars.

1. Observables

Using the matrix U, one can define the correlation matrix $D = UU^\dagger$ with elements $D_{ij} = \langle c_i^\dagger c_j\rangle$, giving us direct access to expectation values. Furthermore, to calculate entanglement entropy S of a bipartition of the system into subsystem A and its compliment B, we restrict D to indices associated with the subsystem A and then diagonalize the restricted matrix to obtain its eigenvalues λ_i. Here, S is then simply given by

$$S = -\sum_i [\lambda_i \ln \lambda_i + (1 - \lambda_i)\ln(1 - \lambda_i)]. \quad \text{(A4)}$$

The connected correlation functions $C(r)$ can be determined from the correlation matrix:

$$C(r) = |D_{i+r,i}|^2 = \langle n_i\rangle\langle n_{i+r}\rangle - \langle n_i n_{i+r}\rangle. \quad \text{(A5)}$$

Similarly, the autocorrelation function $C(\tau)$ can be calculated in the same manner:

$$C(\tau) = |D_{i,i}(t, t + \tau)|^2, \quad \text{(A6)}$$

where $D(t, t + \tau) = U(t + \tau)U^\dagger(t)$.

Finally, one can easily extract the fermion orbitals by taking the columns of U, i.e., $|\psi_i(r)|^2 = |U_{i,r}|^2$. We move the orbitals spatially so that they are centered around the maximum value and then average them over many realizations.

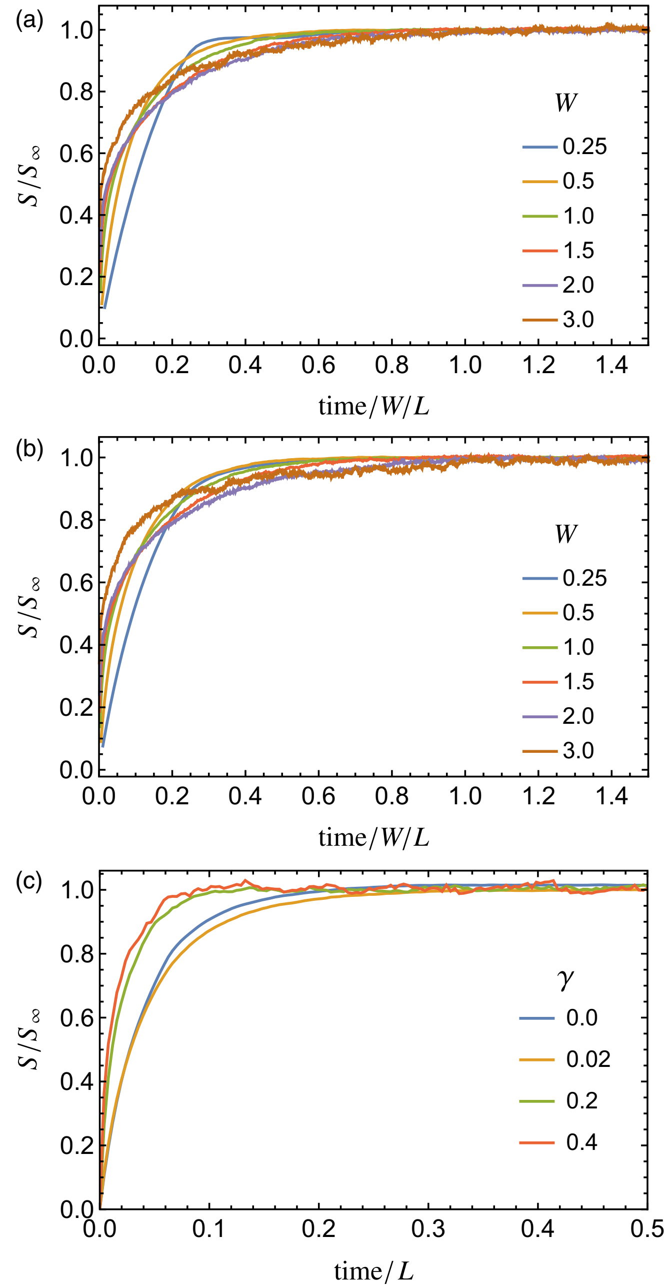

FIG. 8. Time dependence of averaged entanglement entropy S for (a) $\gamma = 0.02$, $L = 256$, (b) $\gamma = 0.02$, $L = 385$, and (c) $W = 0.5$, $L = 256$. The time after which the value reaches saturation value is roughly proportional to the system size L but is also impacted by the disorder strength W and the measurement rate γ.

2. Equilibration to the steady state

The time it takes to reach the steady state is nontrivially dependent on two variables: measurement strength γ and disorder W. In the absence of the disorder, for large γ, we find that the equilibration takes $O(1)$ time, while for small γ, it takes at most $O(L)$ time. Introducing the disorder prolongs the equilibration time roughly proportionally to W (see Fig. 8).

We also note that near $W \approx 2$, the time dependence of the trajectory-averaged half-chain entropy seems to collapse into one curve [see Fig. 9], with the initial behavior scaling as

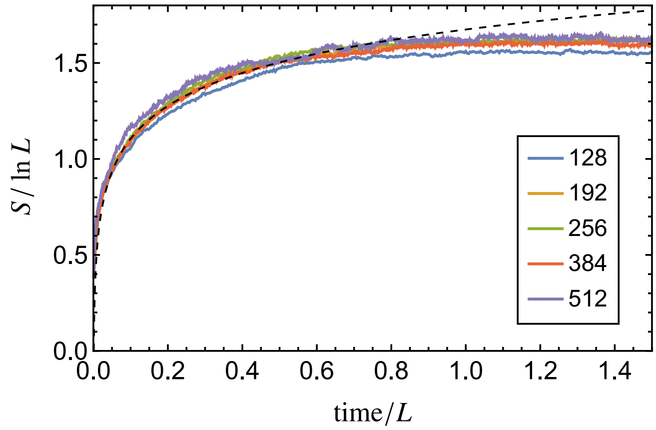

FIG. 9. Emerging conformal symmetry near $W = 2$ for $\gamma = 0.02$. Entanglement entropy is rescaled as $S/\ln L$, while the time is scaled as time$/L$. Dashed line is a fit to a logarithmic behavior.

$S(L/2) \sim \ln(\text{time}/L)$. This suggests an emergence of $z = 1$ conformal symmetry near this point.

3. Finite-size scaling

The data collapse for the finite-size scaling analysis is performed by minimizing the cost function ϵ, which measures how well the data collapse into a single curve given the parameters. First, the data are rescaled using the finite-size scaling *Ansätze* from Eqs. (4) and (5) to produce a set of triples x_i, y_i, d_i representing the rescaled x coordinate, rescaled y coordinate, and the error in the y coordinate. For example, for Eq. (4), $x = (\gamma - \gamma_c^{\bar{S}})(\ln L)^2$, $y = \bar{S}(L/2, L, \gamma) - \bar{S}(L/2, L, \gamma_c^{\bar{S}})$, and d is the error of the half-chain entropy. Then the triples are sorted by their x values, and one can calculate the cost function:

$$\epsilon = \frac{1}{n-2} \sum_{i=2}^{n-1} w(x_i, y_i, d_i | x_{i-1}, y_{i-1}, d_{i-1}, x_{i+1}, y_{i+1}, d_{i+1}), \tag{A7}$$

where

$$w = \frac{(y_i - \bar{y})^2}{\Delta^2}, \tag{A8}$$

$$\bar{y} = \frac{(x_{i+1} - x_i)y_{i-1} - (x_{i-1} - x_i)y_{i+1}}{x_{i+1} - x_{i-1}}, \tag{A9}$$

$$\Delta^2 = d_i^2 + \frac{(x_{i+1} - x_i)^2 d_{i-1}^2 + (x_{i-1} - x_i)^2 d_{i+1}^2}{(x_{i+1} - x_{i-1})^2}. \tag{A10}$$

After obtaining the minimum $\epsilon_{\min}$, one can estimate the error in the collapse parameters by investigating the region where $\epsilon = 2\epsilon_{\min}$.

In Table I, we report the estimates for the parameters from data collapses in Figs. 3, 10, and 11. The scaling function $g(L)$ from Eq. (5) has the following form: $g(L) = [1 + 1/(2\ln L - \beta)]^{-1}$, and can be determined from a superfluid stiffness scaling analogy for the BKT transition [33,131,132].

Supporting data for $W = 0.25$ and $\gamma = 0.04$ are shown in Fig. 10.

TABLE I. Data collapse parameters for the entropy and central charge results.

Data	Entropy $\gamma_c^{\bar{S}}$ or $W_c^{\bar{S}}$	Central charge $\gamma_c^{c(L)}$ or $W_c^{c(L)}$	α	β
$W = 0.0$ [33]	0.31(5)	0.21(5)	3.99	4.37
$W = 0.25$	0.35(5)	0.31(5)	4.00	5.4
$W = 0.5$	0.40(6)	0.35(5)	4.1	7.6
$W = 1.0$	0.33(5)	0.29(5)	5.12	7.65
$\gamma = 0.02$	2.06(15)	1.92(25)	6.4	7.8
$\gamma = 0.04$	2.07(15)	–	–	–

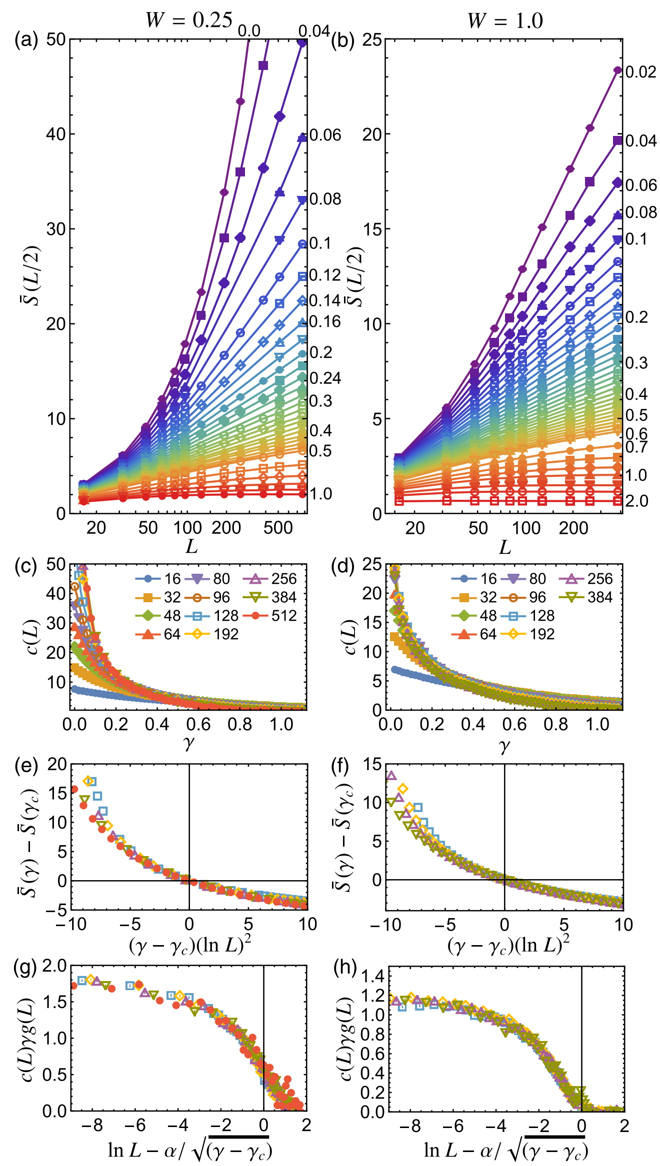

FIG. 10. Behavior of (a) and (b) half-chain entanglement entropy $\bar{S}(L/2)$ for different values of the measurement strength γ (see labels on the right) and (c) and (d) central charge $c(L)$. Data collapse for (e) and (f) $S(L/2)$, and (g) and (h) $c(L)$; legend from (c) and (d) applies in (e)–(h). Left plots are for $W = 0.25$, and the right plots are for $W = 1.0$.

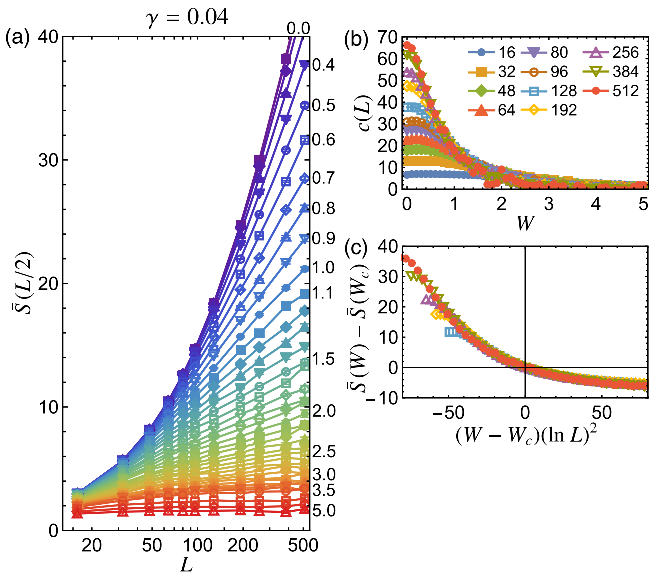

FIG. 11. Results for $\gamma = 0.04$. Behavior of (a) half-chain entanglement entropy $\bar{S}(L/2)$ for different values of W (see labels on the right) and (b) central charge $c(L)$. Data collapse for (c) $S(L/2)$; legend from (b) applies in (c).

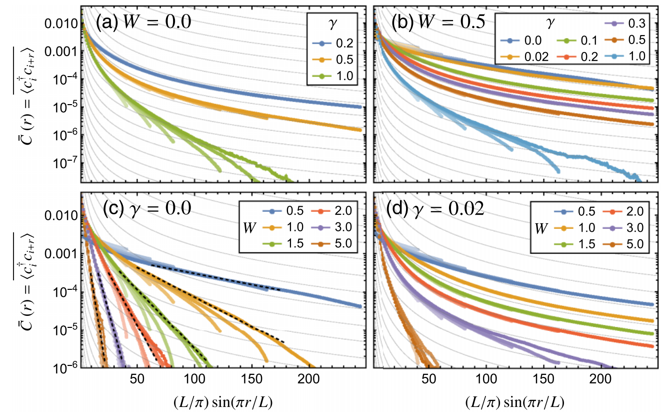

FIG. 12. Connected correlation function $\bar{C}(r)$ for constant disorder strength (a) $W = 0.0$ (no disorder), (b) $W = 0.5$, and constant measurement strength (c) $\gamma = 0.0$, (d) $\gamma = 0.02$. Plot opacity indicates the system size ($L = 128$, 196, 256, 384, 512, and 768). Gray lines show the algebraic decay of $\sim r^{-2}$ expected for the critical phase. Dashed lines in subfigure (c) show exponential decay for Anderson localization.

4. Decay of correlation functions

Although we find that single-particle wave functions are power-law localized, the issue is that these orbitals are not uniquely defined, as the matrix U can be multiplied on the right by any unitary, while not changing the physical state. However, we also find that, for $\gamma > 0$, correlation functions do not seem to exhibit exponential decay (see Fig. 12, where we show the data of Fig. 4 but on a linear-log plot), which would be in agreement with our findings for the orbitals. Perhaps the reason why we do not find scrambled orbitals is due to the uniqueness of the method: both unitary evolution and measurements uniquely transform matrix U (during normalization, QR decomposition is unique as well).

[1] D. M. Basko, I. L. Aleiner, and B. L. Altshuler, Metal-insulator transition in a weakly interacting many-electron system with localized single-particle states, Ann. Phys. **321**, 1126 (2006).

[2] I. V. Gornyi, A. D. Mirlin, and D. G. Polyakov, Interacting electrons in disordered wires: Anderson localization and low-T transport, Phys. Rev. Lett. **95**, 206603 (2005).

[3] A. Pal and D. A. Huse, Many-body localization phase transition, Phys. Rev. B **82**, 174411 (2010).

[4] R. Nandkishore and D. A. Huse, Many-body localization and thermalization in quantum statistical mechanics, Annu. Rev. Condens. Matter Phys. **6**, 15 (2015).

[5] D. A. Abanin, E. Altman, I. Bloch, and M. Serbyn, Colloquium: Many-body localization, thermalization, and entanglement, Rev. Mod. Phys. **91**, 021001 (2019).

[6] Y. Li, X. Chen, and M. P. A. Fisher, Quantum Zeno effect and the many-body entanglement transition, Phys. Rev. B **98**, 205136 (2018).

[7] A. Chan, R. M. Nandkishore, M. Pretko, and G. Smith, Unitary-projective entanglement dynamics, Phys. Rev. B **99**, 224307 (2019).

[8] B. Skinner, J. Ruhman, and A. Nahum, Measurement-induced phase transitions in the dynamics of entanglement, Phys. Rev. X **9**, 031009 (2019).

[9] Y. Li, X. Chen, and M. P. A. Fisher, Measurement-driven entanglement transition in hybrid quantum circuits, Phys. Rev. B **100**, 134306 (2019).

[10] M. Szyniszewski, A. Romito, and H. Schomerus, Entanglement transition from variable-strength weak measurements, Phys. Rev. B **100**, 064204 (2019).

[11] A. Zabalo, M. J. Gullans, J. H. Wilson, S. Gopalakrishnan, D. A. Huse, and J. H. Pixley, Critical properties of the measurement-induced transition in random quantum circuits, Phys. Rev. B **101**, 060301(R) (2020).

[12] J. C. Napp, R. L. La Placa, A. M. Dalzell, F. G. S. L. Brandão, and A. W. Harrow, Efficient classical simulation of random shallow 2d quantum circuits, Phys. Rev. X **12**, 021021 (2022).

[13] R. Fan, S. Vijay, A. Vishwanath, and Y.-Z. You, Self-organized error correction in random unitary circuits with measurement, Phys. Rev. B **103**, 174309 (2021).

[14] M. J. Gullans and D. A. Huse, Dynamical purification phase transition induced by quantum measurements, Phys. Rev. X **10**, 041020 (2020).

[15] A. Bera and S. Singha Roy, Growth of genuine multipartite entanglement in random unitary circuits, Phys. Rev. A **102**, 062431 (2020).

[16] R. Vasseur, A. C. Potter, Y.-Z. You, and A. W. W. Ludwig, Entanglement transitions from holographic

random tensor networks, Phys. Rev. B **100**, 134203 (2019).

[17] Y. Bao, S. Choi, and E. Altman, Theory of the phase transition in random unitary circuits with measurements, Phys. Rev. B **101**, 104301 (2020).

[18] C.-M. Jian, Y.-Z. You, R. Vasseur, and A. W. W. Ludwig, Measurement-induced criticality in random quantum circuits, Phys. Rev. B **101**, 104302 (2020).

[19] A. Zabalo, M. J. Gullans, J. H. Wilson, R. Vasseur, A. W. W. Ludwig, S. Gopalakrishnan, D. A. Huse, and J. H. Pixley, Operator scaling dimensions and multifractality at measurement-induced transitions, Phys. Rev. Lett. **128**, 050602 (2022).

[20] P. Sierant and X. Turkeshi, Universal behavior beyond multifractality of wave functions at measurement-induced phase transitions, Phys. Rev. Lett. **128**, 130605 (2022).

[21] Y. Li, X. Chen, A. W. W. Ludwig, and M. P. A. Fisher, Conformal invariance and quantum nonlocality in critical hybrid circuits, Phys. Rev. B **104**, 104305 (2021).

[22] M. Szyniszewski, A. Romito, and H. Schomerus, Universality of entanglement transitions from stroboscopic to continuous measurements, Phys. Rev. Lett. **125**, 210602 (2020).

[23] J. Lopez-Piqueres, B. Ware, and R. Vasseur, Mean-field entanglement transitions in random tree tensor networks, Phys. Rev. B **102**, 064202 (2020).

[24] O. Shtanko, Y. A. Kharkov, L. P. García-Pintos, and A. V. Gorshkov, Classical models of entanglement in monitored random circuits, arXiv:2004.06736.

[25] A. Lavasani, Y. Alavirad, and M. Barkeshli, Measurement-induced topological entanglement transitions in symmetric random quantum circuits, Nat. Phys. **17**, 342 (2021).

[26] S. Sang and T. H. Hsieh, Measurement-protected quantum phases, Phys. Rev. Res. **3**, 023200 (2021).

[27] L. Zhang, J. A. Reyes, S. Kourtis, C. Chamon, E. R. Mucciolo, and A. E. Ruckenstein, Nonuniversal entanglement level statistics in projection-driven quantum circuits, Phys. Rev. B **101**, 235104 (2020).

[28] S. Choi, Y. Bao, X.-L. Qi, and E. Altman, Quantum error correction in scrambling dynamics and measurement-induced phase transition, Phys. Rev. Lett. **125**, 030505 (2020).

[29] X. Turkeshi, R. Fazio, and M. Dalmonte, Measurement-induced criticality in $(2+1)$-dimensional hybrid quantum circuits, Phys. Rev. B **102**, 014315 (2020).

[30] M. J. Gullans and D. A. Huse, Scalable probes of measurement-induced criticality, Phys. Rev. Lett. **125**, 070606 (2020).

[31] A. Nahum, S. Roy, B. Skinner, and J. Ruhman, Measurement and entanglement phase transitions in all-to-all quantum circuits, on quantum trees, and in Landau-Ginsburg theory, PRX Quantum **2**, 010352 (2021).

[32] X. Cao, A. Tilloy, and A. D. Luca, Entanglement in a fermion chain under continuous monitoring, SciPost Phys. **7**, 024 (2019).

[33] O. Alberton, M. Buchhold, and S. Diehl, Entanglement transition in a monitored free-fermion chain: From extended criticality to area law, Phys. Rev. Lett. **126**, 170602 (2021).

[34] M. Buchhold, Y. Minoguchi, A. Altland, and S. Diehl, Effective theory for the measurement-induced phase transition of Dirac fermions, Phys. Rev. X **11**, 041004 (2021).

[35] C.-M. Jian, B. Bauer, A. Keselman, and A. W. W. Ludwig, Criticality and entanglement in non-unitary quantum circuits and tensor networks of non-interacting fermions, Phys. Rev. B **106**, 134206 (2022).

[36] P. Zhang, C. Liu, S.-K. Jian, and X. Chen, Universal entanglement transitions of free fermions with long-range non-unitary dynamics, Quantum **6**, 723 (2022).

[37] T. Botzung, S. Diehl, and M. Müller, Engineered dissipation induced entanglement transition in quantum spin chains: From logarithmic growth to area law, Phys. Rev. B **104**, 184422 (2021).

[38] X. Turkeshi, A. Biella, R. Fazio, M. Dalmonte, and M. Schiró, Measurement-induced entanglement transitions in the quantum Ising chain: From infinite to zero clicks, Phys. Rev. B **103**, 224210 (2021).

[39] G. Kells, D. Meidan, and A. Romito, Topological transitions with continuously monitored free fermions, SciPost Phys. **14**, 031 (2023).

[40] X. Turkeshi, M. Dalmonte, R. Fazio, and M. Schirò, Entanglement transitions from stochastic resetting of non-Hermitian quasiparticles, Phys. Rev. B **105**, L241114 (2022).

[41] X. Turkeshi, L. Piroli, and M. Schiró, Enhanced entanglement negativity in boundary-driven monitored fermionic chains, Phys. Rev. B **106**, 024304 (2022).

[42] P. Pöpperl, I. V. Gornyi, and Y. Gefen, Measurements on an Anderson chain Phys. Rev. B **107**, 174203 (2022).

[43] M. Ippoliti, M. J. Gullans, S. Gopalakrishnan, D. A. Huse, and V. Khemani, Entanglement phase transitions in measurement-only dynamics, Phys. Rev. X **11**, 011030 (2021).

[44] Y. Bao, S. Choi, and E. Altman, Symmetry enriched phases of quantum circuits, Ann. Phys. **435**, 168618 (2021), special issue on Philip W. Anderson.

[45] Q. Tang and W. Zhu, Measurement-induced phase transition: A case study in the nonintegrable model by density-matrix renormalization group calculations, Phys. Rev. Res. **2**, 013022 (2020).

[46] S. Goto and I. Danshita, Measurement-induced transitions of the entanglement scaling law in ultracold gases with controllable dissipation, Phys. Rev. A **102**, 033316 (2020).

[47] Y. Fuji and Y. Ashida, Measurement-induced quantum criticality under continuous monitoring, Phys. Rev. B **102**, 054302 (2020).

[48] D. Rossini and E. Vicari, Measurement-induced dynamics of many-body systems at quantum criticality, Phys. Rev. B **102**, 035119 (2020).

[49] O. Lunt and A. Pal, Measurement-induced entanglement transitions in many-body localized systems, Phys. Rev. Res. **2**, 043072 (2020).

[50] X. Chen, Y. Li, M. P. A. Fisher, and A. Lucas, Emergent conformal symmetry in nonunitary random dynamics of free fermions, Phys. Rev. Res. **2**, 033017 (2020).

[51] C. Liu, P. Zhang, and X. Chen, Non-unitary dynamics of Sachdev-Ye-Kitaev chain, SciPost Phys. **10**, 048 (2021).

[52] A. Biella and M. Schiró, Many-body quantum Zeno effect and measurement-induced subradiance transition, Quantum **5**, 528 (2021).

[53] S. Gopalakrishnan and M. J. Gullans, Entanglement and purification transitions in non-Hermitian quantum mechanics, Phys. Rev. Lett. **126**, 170503 (2021).

[54] S.-K. Jian, Z.-C. Yang, Z. Bi, and X. Chen, Yang-lee edge singularity triggered entanglement transition, Phys. Rev. B **104**, L161107 (2021).

[55] Q. Tang, X. Chen, and W. Zhu, Quantum criticality in the nonunitary dynamics of $(2+1)$-dimensional free fermions, Phys. Rev. B **103**, 174303 (2021).
[56] X. Turkeshi, Measurement-induced criticality as a data-structure transition, Phys. Rev. B **106**, 144313 (2022).
[57] N. Lang and H. P. Büchler, Entanglement transition in the projective transverse field Ising model, Phys. Rev. B **102**, 094204 (2020).
[58] M. Van Regemortel, Z.-P. Cian, A. Seif, H. Dehghani, and M. Hafezi, Entanglement entropy scaling transition under competing monitoring protocols, Phys. Rev. Lett. **126**, 123604 (2021).
[59] S. Vijay, Measurement-driven phase transition within a volume-law entangled phase, arXiv:2005.03052.
[60] A. Nahum and B. Skinner, Entanglement and dynamics of diffusion-annihilation processes with Majorana defects, Phys. Rev. Res. **2**, 023288 (2020).
[61] Y. Li and M. P. A. Fisher, Statistical mechanics of quantum error correcting codes, Phys. Rev. B **103**, 104306 (2021).
[62] O. Lunt, M. Szyniszewski, and A. Pal, Measurement-induced criticality and entanglement clusters: A study of one-dimensional and two-dimensional clifford circuits, Phys. Rev. B **104**, 155111 (2021).
[63] P. Sierant, M. Schiro, M. Lewenstein, and X. Turkeshi, Measurement-induced phase transitions in $(d+1)$-dimensional stabilizer circuits, Phys. Rev. B **106**, 214316 (2022).
[64] M. J. Gullans, S. Krastanov, D. A. Huse, L. Jiang, and S. T. Flammia, Quantum coding with low-depth random circuits, Phys. Rev. X **11**, 031066 (2021).
[65] L. Fidkowski, J. Haah, and M. B. Hastings, How dynamical quantum memories forget, Quantum **5**, 382 (2021).
[66] T. Maimbourg, D. M. Basko, M. Holzmann, and A. Rosso, Bath-induced Zeno localization in driven many-body quantum systems, Phys. Rev. Lett. **126**, 120603 (2021).
[67] J. Iaconis, A. Lucas, and X. Chen, Measurement-induced phase transitions in quantum automaton circuits, Phys. Rev. B **102**, 224311 (2020).
[68] M. Ippoliti and V. Khemani, Postselection-free entanglement dynamics via spacetime duality, Phys. Rev. Lett. **126**, 060501 (2021).
[69] A. Lavasani, Y. Alavirad, and M. Barkeshli, Topological order and criticality in $(2+1)$D monitored random quantum circuits, Phys. Rev. Lett. **127**, 235701 (2021).
[70] S. Sang, Y. Li, T. Zhou, X. Chen, T. H. Hsieh, and M. P. A. Fisher, Entanglement negativity at measurement-induced criticality, PRX Quantum **2**, 030313 (2021).
[71] B. Shi, X. Dai, and Y.-M. Lu, Entanglement negativity at the critical point of measurement-driven transition, arXiv:2012.00040.
[72] D. Rossini and E. Vicari, Coherent and dissipative dynamics at quantum phase transitions, Phys. Rep. **936**, 1 (2021).
[73] T.-C. Lu and T. Grover, Spacetime duality between localization transitions and measurement-induced transitions, PRX Quantum **2**, 040319 (2021).
[74] M. Ippoliti, T. Rakovszky, and V. Khemani, Fractal, logarithmic, and volume-law entangled nonthermal steady states via spacetime duality, Phys. Rev. X **12**, 011045 (2022).
[75] P. Zhang, S.-K. Jian, C. Liu, and X. Chen, Emergent replica conformal symmetry in non-Hermitian SYK_2 chains, Quantum **5**, 579 (2021).
[76] S.-K. Jian, C. Liu, X. Chen, B. Swingle, and P. Zhang, Measurement-induced phase transition in the monitored Sachdev-Ye-Kitaev model, Phys. Rev. Lett. **127**, 140601 (2021).
[77] G. S. Bentsen, S. Sahu, and B. Swingle, Measurement-induced purification in large-n hybrid Brownian circuits, Phys. Rev. B **104**, 094304 (2021).
[78] T. Minato, K. Sugimoto, T. Kuwahara, and K. Saito, Fate of measurement-induced phase transition in long-range interactions, Phys. Rev. Lett. **128**, 010603 (2022).
[79] E. V. H. Doggen, Y. Gefen, I. V. Gornyi, A. D. Mirlin, and D. G. Polyakov, Generalized quantum measurements with matrix product states: Entanglement phase transition and clusterization, Phys. Rev. Res. **4**, 023146 (2022).
[80] S. Sharma, X. Turkeshi, R. Fazio, and M. Dalmonte, Measurement-induced criticality in extended and long-range unitary circuits, SciPost Phys. Core **5**, 023 (2022).
[81] M. Block, Y. Bao, S. Choi, E. Altman, and N. Y. Yao, Measurement-induced transition in long-range interacting quantum circuits, Phys. Rev. Lett. **128**, 010604 (2022).
[82] T. Müller, S. Diehl, and M. Buchhold, Measurement-induced dark state phase transitions in long-ranged fermion systems, Phys. Rev. Lett. **128**, 010605 (2022).
[83] S. Czischek, G. Torlai, S. Ray, R. Islam, and R. G. Melko, Simulating a measurement-induced phase transition for trapped-ion circuits, Phys. Rev. A **104**, 062405 (2021).
[84] C. Noel, P. Niroula, D. Zhu, A. Risinger, L. Egan, D. Biswas, M. Cetina, A. V. Gorshkov, M. J. Gullans, D. A. Huse *et al.*, Measurement-induced quantum phases realized in a trapped-ion quantum computer, Nat. Phys. **18**, 760 (2022).
[85] P. Sierant, G. Chiriacò, F. M. Surace, S. Sharma, X. Turkeshi, M. Dalmonte, R. Fazio, and G. Pagano, Dissipative Floquet dynamics: From steady state to measurement induced criticality in trapped-ion chains, Quantum **6**, 638 (2022).
[86] R. Medina, R. Vasseur, and M. Serbyn, Entanglement transitions from restricted Boltzmann machines, Phys. Rev. B **104**, 104205 (2021).
[87] U. Agrawal, A. Zabalo, K. Chen, J. H. Wilson, A. C. Potter, J. H. Pixley, S. Gopalakrishnan, and R. Vasseur, Entanglement and charge-sharpening transitions in U(1) symmetric monitored quantum circuits, Phys. Rev. X **12**, 041002 (2022).
[88] Z.-C. Yang, Y. Li, M. P. A. Fisher, and X. Chen, Entanglement phase transitions in random stabilizer tensor networks, Phys. Rev. B **105**, 104306 (2022).
[89] T. Boorman, M. Szyniszewski, H. Schomerus, and A. Romito, Diagnostics of entanglement dynamics in noisy and disordered spin chains via the measurement-induced steady-state entanglement transition, Phys. Rev. B **105**, 144202 (2022).
[90] R. Levy and B. K. Clark, Entanglement entropy transitions with random tensor networks, arXiv:2108.02225.
[91] Y. Minoguchi, P. Rabl, and M. Buchhold, Continuous Gaussian measurements of the free boson CFT: A model for exactly solvable and detectable measurement-induced dynamics, SciPost Phys. **12**, 009 (2022).
[92] G.-Y. Zhu, N. Tantivasadakarn, A. Vishwanath, S. Trebst, and R. Verresen, Nishimori's cat: Stable long-range

entanglement from finite-depth unitaries and weak measurements, arXiv:2208.11136.

[93] G. Piccitto, A. Russomanno, and D. Rossini, Entanglement transitions in the quantum Ising chain: A comparison between different unravelings of the same Lindbladian, Phys. Rev. B **105**, 064305 (2022).

[94] J. Côté and S. Kourtis, Entanglement phase transition with spin glass criticality, Phys. Rev. Lett. **128**, 240601 (2022).

[95] A. Altland, M. Buchhold, S. Diehl, and T. Micklitz, Dynamics of measured many-body quantum chaotic systems, Phys. Rev. Res. **4**, L022066 (2022).

[96] C. Fleckenstein, A. Zorzato, D. Varjas, E. J. Bergholtz, J. H. Bardarson, and A. Tiwari, Non-Hermitian topology in monitored quantum circuits, Phys. Rev. Res. **4**, L032026 (2022).

[97] K. Klocke and M. Buchhold, Topological order and entanglement dynamics in the measurement-only XZZX quantum code, Phys. Rev. B **106**, 104307 (2022).

[98] M. Ippoliti and W. W. Ho, Dynamical purification and the emergence of quantum state designs from the projected ensemble, PRX Quantum **4**, 030322 (2023).

[99] F. Carollo and V. Alba, Entangled multiplets and unusual spreading of quantum correlations in a continuously monitored tight-binding chain, Phys. Rev. B **106**, L220304 (2022).

[100] F. Barratt, U. Agrawal, S. Gopalakrishnan, D. A. Huse, R. Vasseur, and A. C. Potter, Field theory of charge sharpening in symmetric monitored quantum circuits, Phys. Rev. Lett. **129**, 120604 (2022).

[101] F. Barratt, U. Agrawal, A. C. Potter, S. Gopalakrishnan, and R. Vasseur, Transitions in the learnability of global charges from local measurements, Phys. Rev. Lett. **129**, 200602 (2022).

[102] A. Sriram, T. Rakovszky, V. Khemani, and M. Ippoliti, Topology, criticality, and dynamically generated qubits in a stochastic measurement-only Kitaev model, Phys. Rev. B **108**, 094304 (2023).

[103] B. C. Dias, D. Perković, M. Haque, P. Ribeiro, and P. A. McClarty, Quantum noise as a symmetry-breaking field, Phys. Rev. B **108**, L060302 (2023).

[104] A. Milekhin and F. K. Popov, Measurement-induced phase transition in teleportation and wormholes, arXiv:2210.03083.

[105] X. Feng, B. Skinner, and A. Nahum, Measurement-induced phase transitions on dynamical quantum trees, PRX Quantum **4**, 030333 (2023).

[106] S. P. Kelly, U. Poschinger, F. Schmidt-Kaler, M. P. A. Fisher, and J. Marino, Coherence requirements for quantum communication from hybrid circuit dynamics, arXiv:2210.11547.

[107] M. Wampler, B. J. J. Khor, G. Refael, and I. Klich, Stirring by staring: Measurement-induced chirality, Phys. Rev. X **12**, 031031 (2022).

[108] S. Sahu, S.-K. Jian, G. Bentsen, and B. Swingle, Entanglement phases in large-N hybrid Brownian circuits with long-range couplings, Phys. Rev. B **106**, 224305 (2022).

[109] B. Yoshida, Decoding the entanglement structure of monitored quantum circuits, arXiv:2109.08691.

[110] M. Coppola, E. Tirrito, D. Karevski, and M. Collura, Growth of entanglement entropy under local projective measurements, Phys. Rev. B **105**, 094303 (2022).

[111] T. Hashizume, G. Bentsen, and A. J. Daley, Measurement-induced phase transitions in sparse nonlocal scramblers, Phys. Rev. Res. **4**, 013174 (2022).

[112] Y. Li, R. Vasseur, M. P. A. Fisher, and A. W. W. Ludwig, Statistical mechanics model for Clifford random tensor networks and monitored quantum circuits, arXiv:2110.02988.

[113] X. Yu and X.-L. Qi, Measurement-induced entanglement phase transition in random bilocal circuits, arXiv:2201.12704.

[114] T. Kalsi, A. Romito, and H. Schomerus, Three-fold way of entanglement dynamics in monitored quantum circuits, J. Phys. A: Math. Theor. **55**, 264009 (2022).

[115] B. Ladewig, S. Diehl, and M. Buchhold, Monitored open fermion dynamics: Exploring the interplay of measurement, decoherence, and free Hamiltonian evolution, Phys. Rev. Res. **4**, 033001 (2022).

[116] Y. Han and X. Chen, Measurement-induced criticality in $\mathbb{Z}_2$-symmetric quantum automaton circuits, Phys. Rev. B **105**, 064306 (2022).

[117] P. Zhang, Quantum entanglement in the Sachdev-Ye-Kitaev model and its generalizations, Front. Phys. **17**, 1 (2022).

[118] J. M. Koh, S.-N. Sun, M. Motta, and A. J. Minnich, Measurement-induced entanglement phase transition on a superconducting quantum processor with mid-circuit readout, Nat. Phys. **19**, 1314 (2022).

[119] H. Schomerus, Noisy monitored quantum dynamics of ergodic multi-qubit systems, J. Phys. A: Math. Theor. **55**, 214001 (2022).

[120] T. Jin and D. G. Martin, Kardar-Parisi-Zhang physics and phase transition in a classical single random walker under continuous measurement, Phys. Rev. Lett. **129**, 260603 (2022).

[121] Y.-N. Zhou, Generalized Lindblad master equation for measurement-induced phase transition, SciPost Phys. Core **6**, 023 (2023).

[122] T. Iadecola, S. Ganeshan, J. H. Pixley, and J. H. Wilson, Measurement and feedback driven entanglement transition in the probabilistic control of chaos, Phys. Rev. Lett. **131**, 060403 (2023).

[123] M. P. A. Fisher, V. Khemani, A. Nahum, and S. Vijay, Random quantum circuits, Ann. Rev. Condens. Matter Phys. **14**, 335 (2022).

[124] M. Buchhold, T. Müller, and S. Diehl, Revealing measurement-induced phase transitions by pre-selection, arXiv:2208.10506.

[125] Y. Li, Y. Zou, P. Glorioso, E. Altman, and M. P. A. Fisher, Cross entropy benchmark for measurement-induced phase transitions, Phys. Rev. Lett. **130**, 220404 (2023).

[126] Y. Kuno, T. Orito, and I. Ichinose, Purification and scrambling in a chaotic Hamiltonian dynamics with measurements, Phys. Rev. B **106**, 214304 (2022).

[127] Y. L. Gal, X. Turkeshi, and M. Schiro, Volume-to-area law entanglement transition in a non-Hermitian free fermionic chain, SciPost Phys. **14**, 138 (2023).

[128] P. W. Anderson, Absence of diffusion in certain random lattices, Phys. Rev. **109**, 1492 (1958).

[129] D. J. Thouless, A relation between the density of states and range of localization for one dimensional random systems, J. Phys. C: Solid State Phys. **5**, 77 (1972).

[130] E. Abrahams, P. W. Anderson, D. C. Licciardello, and T. V. Ramakrishnan, Scaling theory of localization: Absence of quantum diffusion in two dimensions, Phys. Rev. Lett. **42**, 673 (1979).

[131] K. Harada and N. Kawashima, Universal jump in the helicity modulus of the two-dimensional quantum XY model, Phys. Rev. B **55**, R11949(R) (1997).

[132] J. Carrasquilla and M. Rigol, Superfluid to normal phase transition in strongly correlated bosons in two and three dimensions, Phys. Rev. A **86**, 043629 (2012).

[133] Supporting data for $\gamma = 0.04$ and $W \in \{0.25, 1.0\}$ as well as details of the finite-size scaling analysis and the discussion of single-particle wave functions can be found in Appendix.

[134] I. Poboiko, P. Pöpperl, I. V. Gornyi, and A. D. Mirlin, Theory of free fermions under random projective measurements, arXiv:2304.03138.

[135] M. Kappus and F. Wegner, Anomaly in the band centre of the one-dimensional Anderson model, Z. Phys. B **45**, 15 (1981).

[136] B. L. Altshuler, M. E. Gershenson, and I. L. Aleiner, Phase relaxation of electrons in disordered conductors, Physica E **3**, 58 (1998).

[137] C. W. Kim, J. M. Nichol, A. N. Jordan, and I. Franco, Analog quantum simulation of the dynamics of open quantum systems with quantum dots and microelectronic circuits, PRX Quantum **3**, 040308 (2022).

[138] https://doi.org/10.5522/04/24209346